Journal of Agriculture and Environment for International Development - JAEID 2024, 118 (2): 203-230
DOI: 10.36253/jaeid-15137

Spatial and temporal distribution of infiltration, curve number and runoff coefficients using TOPMODEL and SCS-CN models

MOHAMMAD HOSSEIN PISHVAEI[1], SHABNAM NOROOZPOUR[2], TOORAJ SABZEVARI[1,*], MOSTAFA AKBARI KHEIRABADI[1], ANDREA PETROSELLI[3]

[1]*Department of civil engineering, Estahban Branch, Islamic Azad University, Estahban, Iran*

[2]*Young Researchers and Elite Club, Estahban Branch, Islamic Azad University, Estahban, Iran*

[3] *Department of Agriculture and Forest Sciences (DAFNE), Tuscia University, Viterbo, Italy*

**Correspondence details: tooraj.sabzevari@gmail.com*

Submitted on: 20243, 5 November; accepted on 2024, 15 July. Section: Research Papers

Abstract: Infiltration, the process by which water enters the soil, is intricately intertwined with the attributes of the catchment, including soil composition and vegetation cover, both of which exhibit temporal and spatial variability. Accurate quantification of infiltration rates is imperative for enhancing the predictive capabilities of rainfall-runoff models, especially in regions with limited hydrological monitoring infrastructure, such as many developing countries where a significant portion of catchments remains ungauged. In this study, we integrate the Soil Conservation Service Curve Number (SCS-CN) model with the TOPography-based hydrological MODEL (TOPMODEL) to derive a comprehensive framework for estimating the spatial and temporal dynamics of infiltration and its associated parameters. By leveraging the complementary strengths of these two models, we aim to enhance our understanding of infiltration processes across diverse landscapes. The amalgamation of the SCS-CN model with TOPMODEL Dynamic, which incorporates topographic features, contributing areas, and soil moisture deficit (SMD) dynamics within the watershed, represents a novel approach for characterizing the spatiotemporal variability of infiltration, curve number (CN), and runoff coefficient (RC). This integrated model offers a refined mathematical representation, capable of capturing the intricate interactions between land surface characteristics and hydrological processes, thereby advancing our ability to simulate and predict runoff responses in complex environmental settings.

Keywords: Infiltration, Runoff coefficient, Curve Number, TOPMODEL

Introduction

Rainfall-runoff models have always constituted essential tools in the estimation of flood magnitudes within catchments, particularly in scenarios involving ungauged catchments (Rodriguez-Iturbe and Valdes, 1979, Gupta et al., 1980, Rodriguez-Iturbe et al., 1982; Mesa and Mifflin 1986, Rinaldo et al. 1991, Naden 1992, Rodríguez-Iturbe and Rinaldo, 1997; Sabzevari et al, 2009, Sabzevari, 2010; Sabzevari, 2017, Fariborzi et al., 2019; Petroselli et al., 2020; Adnan et al., 2021a,b; Mohammadpour et al, 2021). These models inherently encompass two fundamental components for determining the temporal distribution of runoff: (i) the conversion of rainfall hyetographs into excess rainfall hyetographs, and (ii) the subsequent transformation of excess rainfall hyetographs into runoff or flow through the catchment, a process commonly referred to as flow routing. Among these components, infiltration plays a pivotal role in rainfall-runoff simulations, as it significantly influences both the timing and magnitude of flow events.

Infiltration rates are affected by numerous factors, including soil composition, vegetative cover, soil moisture content, and rainfall intensity. The accurate estimation of infiltration volumes remains a complex endeavor for hydrologists, primarily due to the heterogeneous temporal and spatial distribution of these factors across catchments (Tricker, 1981; Jaynes & Hunsaker, 1989; Eldridge et al., 2015; Pishvaei et al., 2019). This challenge is particularly pronounced in developing countries, where the application of advanced rainfall-runoff models is hindered by the complexities associated with calibrating numerous input parameters (Ayalew et al., 2022). Under such circumstances, there is a distinct need for rainfall-runoff models characterized by simplicity and parsimony in terms of required input parameters (Petroselli et al., 2020). Moreover, since infiltration changes from one rainfall event to another, this phenomenon changes the runoff and complicates the accurate runoff estimation. Therefore, it is essential to develop simple methods that consider the changes in temporal and spatial patterns of infiltration and its related parameters. This circumstance could be useful not only in hydrology of course, but also, broadly speaking, in terms of management of natural resources, since infiltration affects water availability within soil and this aspect is related for instance to vegetation and biomass growing in hillslopes and in proximity of rivers (Tauro et al., 2016; Apollonio et al., 2021; Crimaldi and Lama, 2021; Lama and Crimaldi, 2121; Lama et al. 2021; Noto et al., 2022; Pirone et al., 2022).

The runoff coefficient (RC), defined as the ratio of cumulative excess rainfall to cumulative total rainfall, stands as a fundamental parameter in hydrology, particularly influential in rational method and water balance computations. Despite its apparent simplicity, the concept of RC continues to hold significance in hydrological designs, serving as a pivotal variable for discerning runoff generation within catchments (Sherman, 1932; Longobardi et al., 2003; Rodriguez et al., 2012). Extensive investigations have been undertaken to elucidate the influence of physiographic, hydrological, climatic, and geological factors on RC (Betson & Blaes, 1981; Boughton, 1987; Gottschalk & Weingartner, 1998; Castro et al., 1999; Longobardi et al., 2003; Cerdan et al., 2004; Merz et al., 2006; Carrillo et al., 2006; Patil and Bardossy, 2006; Merz & Bloschl, 2009; Visessri & McIntyre, 2016).

Merz et al. (2006) investigated spatio-temporal variations in RC utilizing hourly data encompassing rainfall, snow, and runoff from 50,000 events across 337 Austrian catchments spanning areas of 80 to 10,000 km2 between 1981 and 2000. Their findings highlighted correlations between the spatial distribution of RC and mean annual rainfall, with slight associations observed between RC and soil type/land use. Bales and Betson (1981) demonstrated the high sensitivity of runoff depth to changes in the Curve Number (CN) value, an empirical parameter introduced by the Soil Conservation Service (SCS) characterizing the rainfall-infiltration relationship. Moreover, they emphasized the significance of land use and soil physical properties in determining CN values based on analysis of 585 observed floods across 36 catchments. Patil and Bardossy (2006) conducted a regional analysis of RC considering climatic attributes within Australian catchments, concluding significant relationships between average annual rainfall, soil antecedent moisture, and evapotranspiration, while observing non-significant associations with land use, soil type, and geology.

In a similar vein, Visessri and McIntyre (2016) scrutinized regional RC across 44 gauged sub-catchments in Northern Thailand, focusing on the impacts of land use and antecedent moisture conditions. Their study highlighted the successful regionalization of the runoff coefficient, albeit with weaker associations observed for the base flow index and seasonal elasticity. Notably, they identified significant non-stationarity within both flow response and land use indices.

To investigate the spatial and temporal dynamics of infiltration, excess rainfall, and RC within catchments, it becomes imperative to employ rainfall-runoff models capable of incorporating these intricate characteristics. Thus, this research endeavors to utilize a combination of the Soil Conservation Service Curve Number (SCS-CN) and TOPMODEL models.

The SCS-CN model, predicated on the principle that excess rainfall is always less than or equal to total rainfall (Chow, 1964), necessitates the determination of the CN, assumed to be a function of soil properties, land use, and soil antecedent moisture. Its simplicity has rendered it a favored method among engineers and experts (McCuen, 1982; Michel et al., 2005; Mishra et al., 2006; Singh et al., 2010; Apollonio et al., 2018).

Conversely, TOPMODEL, a widely employed rainfall-runoff model, utilizes topographic information to compute catchment runoff, employing the concept of the Topographic Wetness Index (TWI) to delineate the spatial distribution of contributing areas at each time step. Additionally, it accounts for SMD, which impacts infiltration, until reaching saturation. This model has found application in deriving soil moisture maps and estimating subsurface flow and erosion within catchments (Montgomery & Dietrich, 1994; Woods et al., 1997; Western et al., 1999; Wang et al., 2010).

Efforts have also been made to integrate TOPMODEL with geographic information system (GIS), mainly from a hydrological perspective (e.g. Chairat & Delleur, 1993; Stuart & Stocks, 1993). Previous research on predicting soil moisture using TOPMODEL is either using topographic indices to predict soil moisture distribution patterns or using the simulated SMD to predict the water tables or groundwater (Quinn, & Beven, 1993; Lamb et al., 1997). Furthermore, TOPMODEL is used in GIS frameworks for flood predictions (Li & Zhang, 2008; Nourani & Mano, 2007; Takeuchi et al., 2008).

Saturation excess, a hydrological phenomenon occurring when soil layers become fully saturated, impeding further infiltration, is typically associated with prolonged, gentle-to-moderate rainfall events. A series of researches in the past have dealt with the relationship between SCS and TOPMODEL models. In their research, the concept of excess saturation and its relationship with the SCS model was mentioned (Takeuchi et al., 1999; Shokoohi, 2016; Sisi et al., 2017; Azizian and Shokoohi, 2019; Pishvaei et al., 2019; Nguyen and Christophe Bouvier, 2019; Panjabi et al., 2020). Shokoohi (2016) conducted a comprehensive review assessing the influence of different sources used to prepare digital elevation models on the TWI and subsequently evaluated the performance of TOPMODEL. Azizian and Shokoohi (2019) proposed a novel method leveraging the saturation excess concept to estimate the CN of a catchment. Their approach facilitated the determination of a CN value based on the Dunne-Black mechanism, wherein subsurface flow dynamics significantly affect CN values. Through empirical equations based on soil porosity, average distance to subsurface water level, and a parameter controlling the effective depth of saturated soil, they demonstrated the utility of saturation excess in accurately estimating CN values in the Kasilian basin, Iran.

Pishvaei et al. (2019) investigated the influence of hillslope topography on the spatial distribution of infiltration and excess rainfall using TOPMODEL and SCS-CN models. They extended SMD estimation equations to account for complex hillslope geometries and evaluated the effects of topography on SMD and infiltration. Their findings indicated that hillslope plan shape exerted a significant influence on infiltration, excess rainfall, and runoff, with convergent hillslopes exhibiting lower infiltration rates and higher runoff compared to other geometries.

Despite these advancements, research pertaining to the evaluation of spatial and temporal infiltration distribution remains scarce. In the present study, we developed novel equations by coupling the SCS-CN and TOPMODEL models based on the Dunne-Black mechanism. These equations enable the characterization of spatial and temporal variations in critical hydrological parameters related to infiltration derived from the SCS infiltration model. Employing GIS, we extracted information from a case study (the Kasilian catchment in Iran) to analyze and assess the spatial distribution of CN, infiltration, and RC within the catchment. Subsequently, laboratory experiments were conducted to investigate temporal variations in CN, infiltration, and RC. Finally, simulated hydrographs obtained from the new equations were compared with observed hydrographs.

Our research hypotheses posit that the presence of near-surface bedrock in hillslopes facilitates rapid subsurface flow formation during rainfall infiltration, thereby characterizing runoff mechanisms akin to the Dunne-Black type. While both the SCS-CN and TOPMODEL methods offer distinct advantages, each also presents limitations when used in isolation. The high dependency of the SCS-CN method on the CN parameter, influenced by factors such as land slope and topography, underscores the need for coupling these models to mitigate inherent limitations (Soomro et al., 2019; Faouzi et al., 2022). Integration of the TOPMODEL's topography index with the SCS-CN model holds promise in addressing these challenges effectively.

The primary objectives of this research encompass the following key aims:

1. Integration of the TOPMODEL subsurface model with the SCS-CN infiltration model, culminating in the development of a novel, straightforward methodology for examining spatial infiltration patterns within catchments.

2. Utilization of ArcGIS to compute spatial infiltration and runoff coefficient values within the Kasilian catchment, thereby facilitating a comprehensive analysis of hydrological processes at the spatial scale.

3. Application of both Dynamic TOPMODEL and the SCS-CN infiltration model, in conjunction with a laboratory model, to compute spatial and temporal infiltration dynamics within the catchment. This multifaceted approach enables a nuanced understanding of both the spatial distribution and temporal evolution of infiltration processes, thereby enhancing insights into catchment hydrology.

Materials and Methods

TOPMODEL description

TOPMODEL is a rainfall-runoff model in which topographic properties of the hillslope and contributing areas play a major role in predicting runoff. The topographic information used in this model is incorporated in the TWI that is defined as:

$$\lambda = ln\left[\frac{a}{tan\,\beta}\right]\lambda \qquad (1)$$

In the given equation, λ represents the TWI, a parameter crucial for delineating hydrological flow patterns within a catchment. The term a denotes the specific catchment area, indicative of the total area contributing flow to a given point within the catchment. Additionally, the tangent of the slope angle, denoted as tanβ, quantifies the portion of flow capable of traversing through the point under the influence of gravitational forces. These components are visually illustrated in Figure 1 for enhanced clarity and understanding.

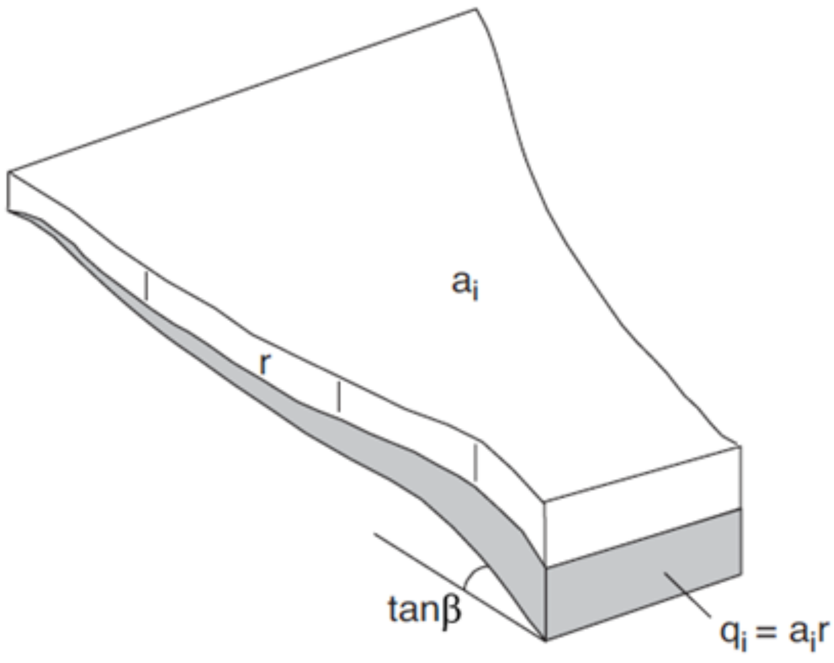

Figure 1 - Specific catchment area (drainage area: ai) and slope angle (β) in TOPMODEL (qi is subsurface flow; r is recharge rate) (Beven, 2011)

The TWI serves as a critical indicator of flow accumulation tendencies across hillslopes. In Figure 1, consider point i at the outelet of the hillslope. The saturation rate index (TWI) at point i depends on the amount of subsurface flow entering this point (qi), which is a function of the area upstream of the hillsope at this point (a) and the amount of drainage at this point is a function of the local slope (tan β). The higher the subsurface flow and the lower the slope, the higher the TWI value.

If the discharge is low and the subsurface flow is high, that element will be saturated sooner. In regions characterized by steep slopes, particularly within hilly catchments where specific catchment area (a) values are minimal, TWI values tend to be correspondingly low. Conversely, in flat or plain regions characterized by higher specific catchment area values and lower slope gradients, TWI values exhibit an upward trend, indicating an increased propensity for flow accumulation.

The main TOPMODEL equation is presented as

$$\boldsymbol{D_i = \overline{D} - m[\lambda(i) - \overline{\lambda}]D_i} \qquad (2)$$

where D_i represents the soil moisture deficit (SMD) to saturated condition at point i, $\overline{D}$indicates the mean soil moisture deficit, and $m = \Theta_e / f$, with Θ_e being the effective *s*oil moisture and parameter f demonstrating how the hydraulic conductivity decreases with depth. Usually, the parameter $\overline{D}$ and f are calibrated based on the observed runoff hydrograph. First, initial values are considered for parameters and the calculated flow rate at the outlet of the catchment is matched to the observed flow hydrograph by trial and error technique. In Eq. (2), $\lambda(i)$ is the TWI, and is calculated from Eq. (3) for each point i along the flow path:

$$\boldsymbol{\lambda(i) = ln\left[\frac{a(i)}{s(i)}\right]} \qquad (3)$$

The parameter a represents the specific catchment area (SCA), the value of which at each point i is equal to the contributing drainage area, Ai, per flow width, bi, at that point (Figure 2).

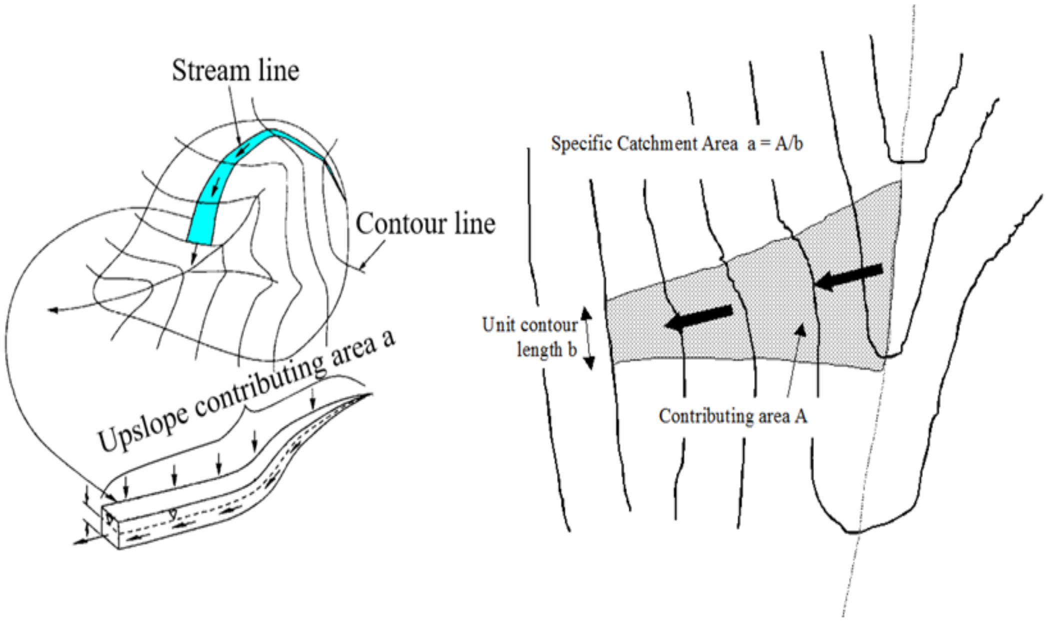

Figure 2 - The ratio of the upstream catchment area to the flow width (SCA) (Sabzevari, 2010).

It should be noted that $\overline{\lambda}$ represents the areal average λ over the hillslope area, which is calculated as follows:

$$\overline{\lambda} = \frac{\int_0^L ln\left[\frac{a(i)}{s(i)}\right] w(i)\mathrm{di}}{\int_0^L w(i)\mathrm{di}} \tag{4}$$

$w(i)$ is the width of the hillslope at any point, the terms $\overline{\lambda}$ and λ can be obtained from topographic maps and digital elevation model (DEM) and are a function of the topographic characteristics of the hillslopes.

SCS-CN infiltration model

The Soil Conservation Service (1972) developed an experimental infiltration model (SCS-CN) to calculate runoff depth from rainfall. Initially, this method was used only in small and agricultural catchments and then it was extensively applied in larger catchments. The balance equation, as the basis of this model, is defined as follows:

$$P = Ia + F + R \tag{5}$$

where R represents the amount of excess rainfall, F indicates the cumulative infiltration, P is the total rainfall depth, and I_a is the initial loss. With the assumption that the ratio of the runoff rate to the rainfall is equal to the ratio of real storage to potential storage, Eq. (5) can be written as:

$$\frac{R}{P-Ia} = \frac{F}{S} \tag{6}$$

where S is the potential maximum soil moisture retention and depends on factors such as vegetation cover, soil type, and soil moisture condition. The collection of these factors is summarized in the CN parameter. The parameter S is calculated as follows:

$$S = \frac{1000}{CN} - 10 \tag{7}$$

in which the value of CN varies theoretically from 0 to 100. It should be noted that the value of *S* is in inches in this equation. As aforementioned, the value of CN is equal to 100 when the surface is completely impervious while this parameter is 0 when the rainfall infiltrates totally within the soil. By combining Eqs. (5) and (6), it is possible to obtain Eq. (8):

$$R = \begin{cases} \frac{(P-I_a)^2}{(P-I_a+S)} & P > I_a \\ 0 & P \le I_a \end{cases} \tag{8}$$

Considering the guidelines of the SCS, if Ia = 0.2S then the runoff depth is calculated as follows:

$$R = \begin{cases} \frac{(P-0.2S)^2}{P+0.8S} & P > I_a \\ 0 & P \le I_a \end{cases} \tag{9}$$

Equation (9) represents the fundamental excess rainfall equation within the SCS-CN model, enabling the computation of direct runoff volumes within a given catchment. This equation accounts for the dynamic variations in infiltration rates over time during rainfall events. The cumulative infiltration can be derived from Equation (10) by integrating the terms $F_t = F + I_a$ and combining Eqs. (6) and (8):

$$F_t = P - R = \begin{cases} \frac{S(P-0.2S)}{(P+0.8S)} + 0.2S & P > 0.2S \\ P & P \le 0.2S \end{cases} \tag{10}$$

Spatial changes of infiltration

This section combines TOPMODEL and SCS-CN equations and provides relationships to consider spatial and temporal changes of parameters such as SMD, infiltration, CN, and RC in a catchment. Figure 3 shows a hillslope with a subsurface flow. If the distance of the groundwater table to the land surface is at the point *i* of the hillslope z_i, the amount of soil moisture deficit to saturated condition is $D_i = \theta_i z_i$ (Beven et al., 1995) (Θ_i is initial soil moisture). If the subsurface water table level is the same as the ground level at a point in the hillslope, this point will be a point of the saturated level.

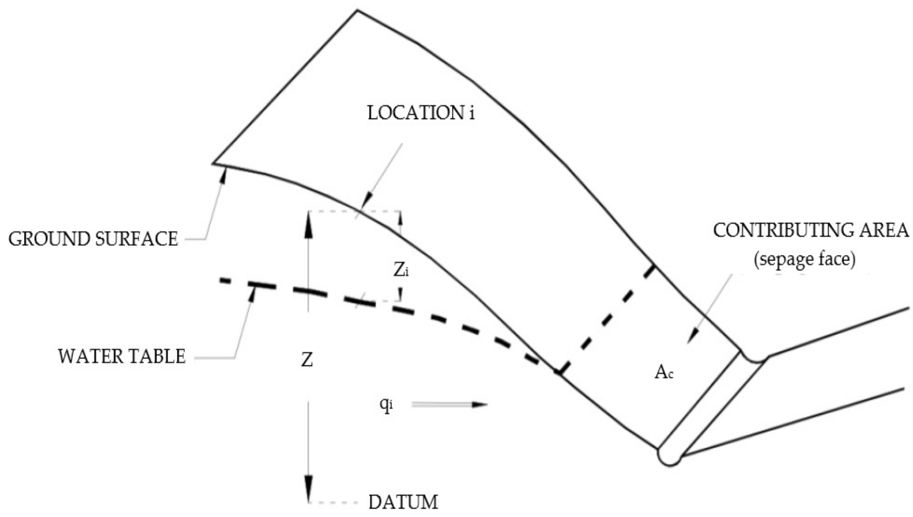

Figure 3 - Schematic representation of a valley and runoff formation according to the TOPMODEL. Ac: contributing area to the surface runoff; qi: interflow corresponding to an area drained per unit contour length. (Sivapalan et al., 1987).

Where qi is subsurface flow, Ac is seepage face. The value of zi in Figure 3 indicates the distance from the water table elevation, as well as the remaining capacity to reach the saturation level. In other words, the parameter zi represents the moisture deficit to saturated condition and the potential for water retention in the soil. The higher the values of zi, the higher water retention potential of the cell. In saturated condition, where the parameter zi is equal to zero, the amount of soil retention capacity and moisture deficit to saturated level are also zero.

According to Eq. (7) in the SCS-CN model, the maximum infiltration value at any point equals $S = (\frac{1000}{CN} - 10) \times 25.4$ (in mm). In this study, the value of SMD at each point is considered equal to the value of S at that point (Nachabe, 2006; Azizian and Shokoohi, 2019; Pishvaei et al., 2019). Thus, the spatial variation of SMD can be expressed based on Eq. (11):

$$D_i = S_i = (\frac{1000}{CN_i} - 10) \times 25.4 \qquad (11)$$

In Eq. (11), the maximum infiltration at any point (*S*) is practically considered equal to soil moisture deficit at that point. Thus, the value of the curve number at each point *i* is calculated by Eq. (12) as follows:

$$CN_i = (\frac{25400}{D_i + 254}) \qquad (12)$$

Eq. (12) indicates the spatial changes of the curve number parameter along the hillslope. If the value of D_i obtained from Eq. (12) is substituted in Eq. (10), then the amount of cumulative infiltration for each point *i* is calculated as follows:

$$F_t = \begin{cases} \frac{D_i(P - 0.2D_i)}{P + 0.8D_i} + 0.2D_i & P > 0.2D_i \\ P & P \le 0.2D_i \end{cases} \qquad (13)$$

where P represents the cumulative rainfall and F_t indicates the cumulative infiltration during rainfall. Since the parameter D_i is a function of the location of the point, Eq. (13) determines the spatial distribution of infiltration. Considering the infiltration values, the value of RC in each element is calculated by Eq. (14) and its average value from Eq. (15) (Franchini et al., 1996):

$$RC_i = c_i = 1 - \frac{Fi}{P} \tag{14}$$

$$\overline{c} = \frac{\sum C_i w_i \Delta x}{\sum w_i . \Delta x} = \frac{\sum C_i w_i}{\sum w_i} \tag{15}$$

By using Eqs. (14) and (15), it is possible to determine the spatial changes of infiltration and RC at any desired distance i from the upstream of the hillslope.

Temporal changes of infiltration (Dynamic TOPMODEL)

In addition to spatial changes of infiltration, the pattern of temporal changes in infiltration is also very important in estimating surface and subsurface flow. In this section, by combining the balance equations of TOPMODEL and SCS-CN, equations are presented that can consider the time changes of the important parameters of infiltration like SMD, curve number and runoff coefficient.

The parameter $\overline{D}$ in Eq. (2) indicates the average value of SMD. The value of $\overline{D}$ is updated at every Δt on the basis of the following equation (Franchini et al., 1996):

$$\overline{D}^{(t+1)} = \overline{D}^{(t)} - \left[\frac{Qv^{(t)} - QB^{(t)}}{A}\right] \Delta t \tag{16}$$

Equation 16 calculates the $\overline{D}$ values in each time step based on the balance equation. Where Q_v is the recharge rate of the saturated zone over the time interval t, Q_B is the outflow from the subsurface store into the channel over the time interval t and $t+\Delta t$, A is the area of the hillslope, and Δt is the time interval.

The quantity Q_B can be defined analytically as Eq. (17):

$$Q_B^{(t)} = \int_L T_0 \tan\beta \, exp(-\frac{Di^{(t)}}{m}) dL \tag{17}$$

where L is twice the length of all stream channels. Bearing in mind Eq. (2), $Q_B{}^{(t)}$ can be written as Eq. (18):

$$Q_B^{(t)} = \int_L T_0 \tan\beta \, exp(-\frac{\overline{D}i^{(t)}}{m} - \overline{\lambda} + Ln\frac{a}{\tan\beta}) dL = T_0 \tan\beta \, exp(-\frac{\overline{D}i^{(t)}}{m}) \int_L a dL \tag{18}$$

Because

$$\int_L a dL = A(total\ area\ of\ basin) \tag{19}$$

Then

$$Q_B^{(t)} = AT_0\, exp(\overline{\lambda})\, exp(\frac{-\overline{D}^{(t)}}{m}) = Q_0\, exp(\frac{-\overline{D}^{(t)}}{m}) \qquad (20)$$

With $Q_0=AT_0 \exp\overline{\lambda}$.

The recharge Q^t_v can be represented as the sum of the contribution of all the grid squares covering the basin (these grids are those of the DEM used to define the index curve):

$$Qv^{(t)} = \sum_{i\in A} Qv_i{}^{(t)} = \sum \alpha i\, K_0\, exp(\frac{-\overline{D}^{(t)}}{m}) \quad for \quad Di \geq 0 \qquad (21)$$

where α_i is the area of the i[th] grid square. The equation assumes that the transfer from the unsaturated to the saturated zone is controlled by the conductivity at the depth of the 'perched water table', under unit vertical hydraulic gradient (Beven, 1986a). Naturally, Eq. (21) holds good when the current water content in the unsaturated zone is not a limiting factor; otherwise, the contribution is calculated on the basis of the actual amount of water available. Lastly, it is worth stressing that Eq. (21) extends to all the grids where $D_i \geq 0$.

The continuity equation (16) is initialized by assuming that the simulation begins after a long dry period; in other words, the unsaturated zone is held to be totally dry and the flow observed at the basin outlet is deemed to have been generated only by the subsurface flow contribution: $Qv^{(1)} = 0$, $Q_B^{(1)} = Q_0 B^{(1)}$

Recalling Eq. (20), $Q_B{}^1$ may be written as

$$Q_B^{(1)} = Q_0\, exp(\frac{-\overline{D}^{(t)}}{m}) \qquad (22)$$

and therefore, the initial state is:

$$\overline{D}^{(1)} = -mLn(\frac{Q_{0b}^1}{Q_0}) \qquad (23)$$

With Eq. (2) it is possible to define the initial depth of the perched water table in each grid square.

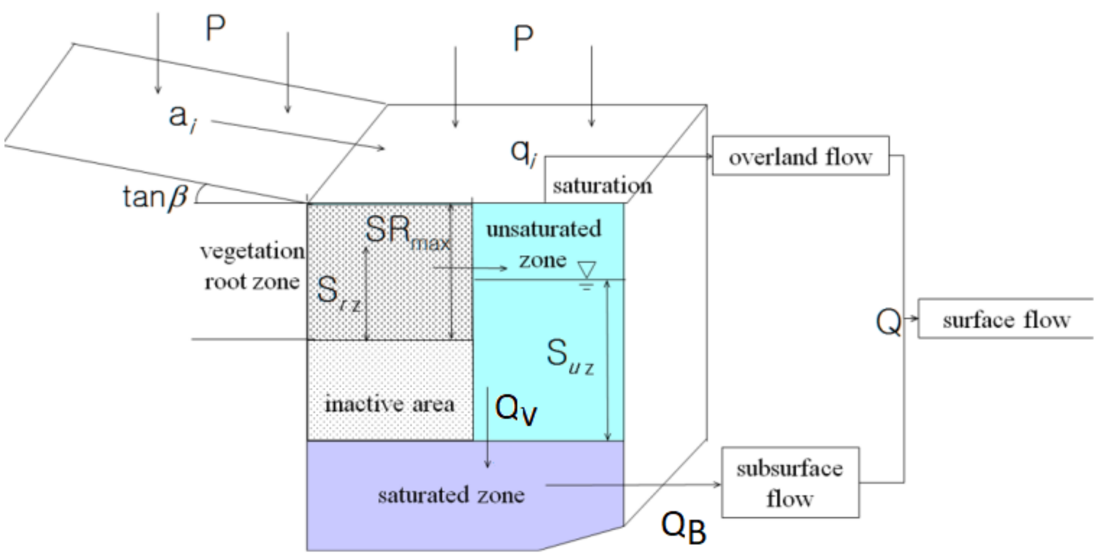

Figure 4 - Basic concept of the TOPMODEL scheme (Franchini et al, 1996).

Where K_0 is the hydraulic conductivity coefficient at the ground surface, $T_0 = K_0 / f$ is the soil transmissivity, f is the decay factor, α_i is the area draining through location i per unit contour length (i.e. the contributing area at point i). Figure 5 depicts the discretization of a rectangular hillslope. This hillslope with the length L is divided into n parts with the width Δx. The area of each part (α_i) is the width w of the part multiplied by Δx, which is selected based on changes in hillslope characteristics.

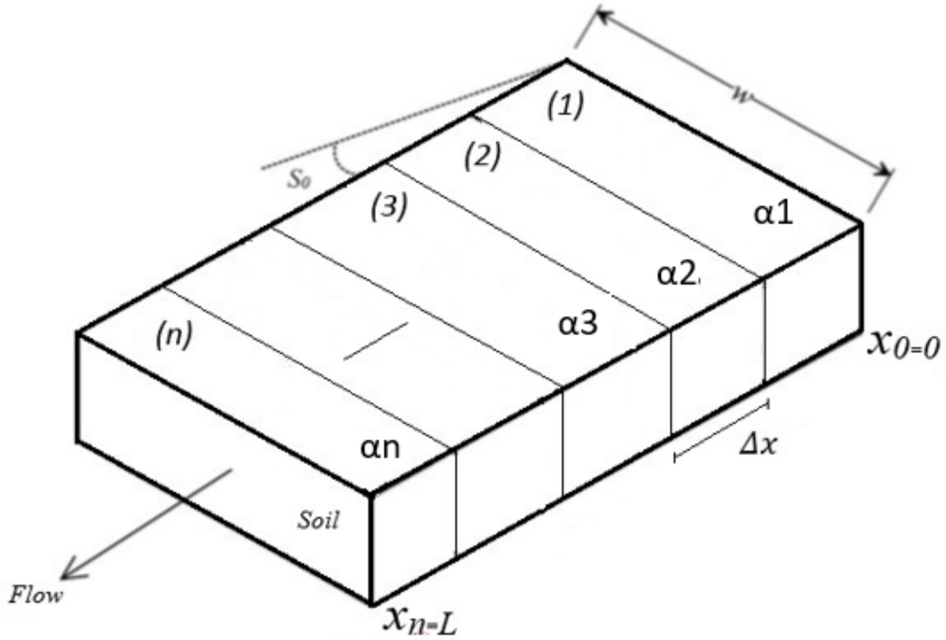

Figure 5 - Spatial discretization of the hillslopes

By calculating $\overline{D}$ from Eq. (16) and substituting it in Eq. (2), it is possible to calculate the values of D_i for each time step. In this way, knowing the values of temporal variation D_i allows calculating the temporal variation of RC. However, RC is practically determined as a percentage of rainfall that is converted to runoff, and then, the runoff depth is estimated by the simple formula R = RC* P, in which R represents the runoff depth, RC is the runoff coefficient, and P is the rainfall depth. By combining Eqs. (7) and (9), RC is calculated according to Eq. (24):

$$c = \frac{R}{P} = \frac{(P - 0.2\times(\frac{1000}{CN} - 10))^2}{P(P + 0.8\times(\frac{1000}{CN} - 10))} \quad (24)$$

Eq. (24) illustrates that RC is a function of rainfall depth (in inches) and CN. Further, this equation provides an analytical solution for CN in the form of Eq. (25):

$$CN = (0.005P + 0.01cP + 0.005P(c(4c+5))^{0.5} + 0.01)^{-1} \quad (25)$$

According to Eq. (2), the values of D_i can be calculated in each pixel of the hillslope (spatial) and in each time step. If the value of the infiltration depth is indicated by the parameter F for a given rainfall depth P, then, three conditions can be considered as follows: If $D_i \geq 0$, then the pixel i is saturated. In this case, $F = 0$ and all rainfall P is converted to runoff. Furthermore, RC is equal to 1 and runoff volume is calculated by Eq. (26):

$$V = P \times \alpha_i \tag{26}$$

b) If $D_i \geq F$, then pixel i is unsaturated and does not contribute to runoff generation. In this case, $F = P$ and the RC is equal to 0.

c) If $0 < D_i < F$, then pixel i is semi-saturated. In this case, the α portion of rainfall is converted into runoff and the remaining portion infiltrates. Therefore, RC is between 0 and 1, and the runoff volume is calculated from Eq. (27).

$$V = R \times \alpha_i = (P - D_i) \times \alpha_i \tag{27}$$

Furthermore, the amount of infiltration depth and RC for each pixel i at each time step can be calculated from Eqs. (28) and (29) as follows:

$$F_i^{(t)} = P_i^{(t)}(1 - c_i^{(t-1)}) \tag{28}$$

$$c_i^{(t)} = \frac{F_i^{(t)} - D_i^{(t)}}{P} \tag{29}$$

Under the initial conditions, it is assumed that all the rainfall infiltrates (P = F).

By combining Eq. (25) and (29), the value of the CN parameter in each time and spatial step is calculated from Eq. (30) (Ou, 2009 & Wolock, 1993):

$$CN_i^t = (0.005P_i^t + 0.01c_i^tP_i^t + 0.005P_i^t(c_i^t(4c_i^t + 5))^{0.5} + 0.01)^{-1} \tag{30}$$

Eqs. (29) and (30), which are among the achievements of this research, provide the possibility to determine the temporal and spatial distribution of two important hydrological parameters (RC and CN). In fact, the values of $\overline{D}$ are calculated for each time step based on Eq. (16) and then, the parameter D_i is determined in each pixel and the calculations are repeated.

In TOPMODEL, the direct runoff is calculated from Eq. (31):

$$Q_{dir} = \sum_A a_i I_i \;\; for \;\;\; Di \leq 0 \tag{31}$$

Where I is the rainfall intensity. According to Eq. (31), the direct runoff is generated in the saturated pixels (either the pixel has already been saturated in previous time steps or is saturated during the current time steps).

The study area

To operationalize the two proposed models within this study, two distinct study were devised. This section deals with the first case study, i.e. the integration of TOPMODEL with Geographic Information Systems (GIS), that can facilitate a comprehensive analysis of spatial variations in infiltration and associated parameters. Consequently, the dataset pertaining to the Kasilian watershed in Iran was leveraged to conduct this investigation, enabling a detailed exploration of infiltration dynamics within the region. The study area is the Kasilian catchment, with an area of 66.75 km^2. This catchment lies in a geographical location between 30″58’35° to 36″07’36° north latitude and 44″08’53° to 42″15’53° east longitude, in northern Iran and south of the Caspian Sea. The elevation range of this catchment is between 1100 and 3158 m, with an average of 1576 m above sea level and annual average precipitation of 800 mm (Figure 6).

Land use of Kasilian watershed mainly includes forests, pastures, agriculture, residential and rock outcrops. Most of the soil in the catchment is sandy clay.

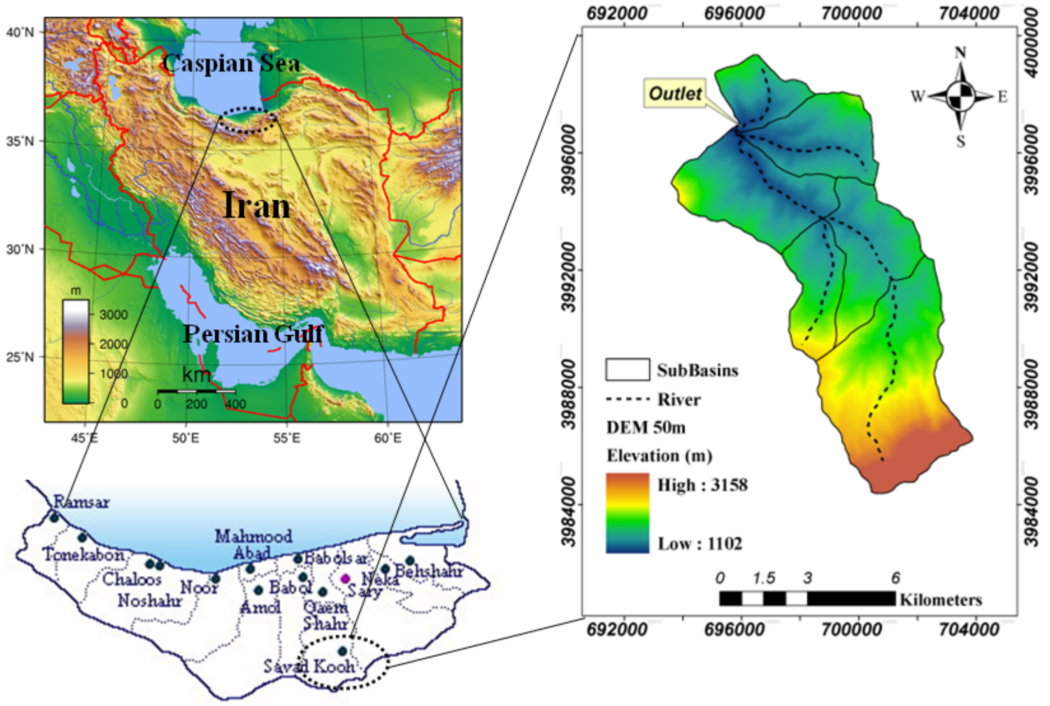

Figure 6 - Location and general data of Kasilian catchment. From (Sabzevari, 2010).

The Laboratory model

Regarding the second protocol, dynamic TOPMODEL model is used to investigate spatial-temporal infiltration. Due to the fact that GIS considers spatial changes, it was not possible to use this model in the Kasilian catchment in this research, so the information from a laboratory model was used.

Temporal variations in infiltration, RC, and CN were investigated using a laboratory model, as depicted in Figure 7. This laboratory setup was designed to simulate the hydrograph of surface and subsurface flows across hillslopes with varying slopes. To achieve this, a rainfall simulator was incorporated into the laboratory model, enabling the generation of rainfall events with differing intensities. Table 1 provides a comprehensive overview of the laboratory model specifications utilized in this study. The dimensions of the soil reservoir are detailed, with a length of 192 cm, a width of 100 cm, and a depth of 35 cm. The hydraulic conductivity of the soil within the laboratory setup was determined to be 3.67 cm/hr. Additionally, surface and subsurface flows were quantified separately using two distinct weirs, facilitating accurate measurement of flow rates. These data were instrumental in assessing the temporal evolution of infiltration time, RC, and CN dynamics within the experimental framework.

Table 1 - Geometric characteristics and soil of the studied hillslope on a laboratory scale

Characteristics	Symbol	Unit	Value
Length	L	m	1.9
Width	*w*	m	1
Slope	*s*	degree	9
Soil hydraulic conductivity	K_0	m/hr	0.036
Decay factor	*f*	-	30
Porosity	*n*	-	0.437

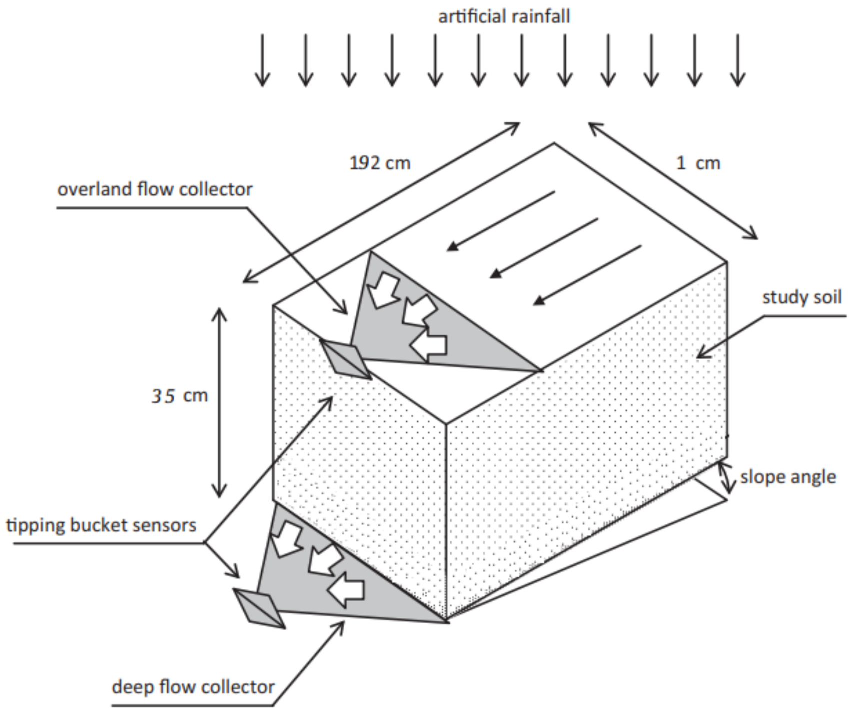

Figure 7 - Schematic of hydrological rain simulator

Results and Discussion

Spatial changes in infiltration (Kasilian catchment)

Figure 8 shows the GIS data of the Kasilian catchment, including DEM information, flow direction, and slope.

Regarding the geomorphological information of the catchment, the values of $\lambda(i)$ are calculated from Eq. (3) for each pixel of the hillslope, and then SMD values are determined from Eq. (16). Figure 9 displays the changes in these two parameters in the Kasilian catchment. It should be noted that λ and SMD are independent of rainfall and are a function of the geometric characteristics of the catchment.

As illustrated in Figure 9, regions characterized by high slopes and/or low contributing areas exhibit low values of the TWI (λ), accompanied by SMD values approaching unity. In contrast, areas with low slope gradients tend to manifest elevated λ values. Notably, an inverse relationship between λ(x) and SMD is observed, indicative of soil saturation tendencies near stream channels where SMD values tend towards zero. This relationship underscores the influence of local topographic and hydrological conditions on soil moisture dynamics.

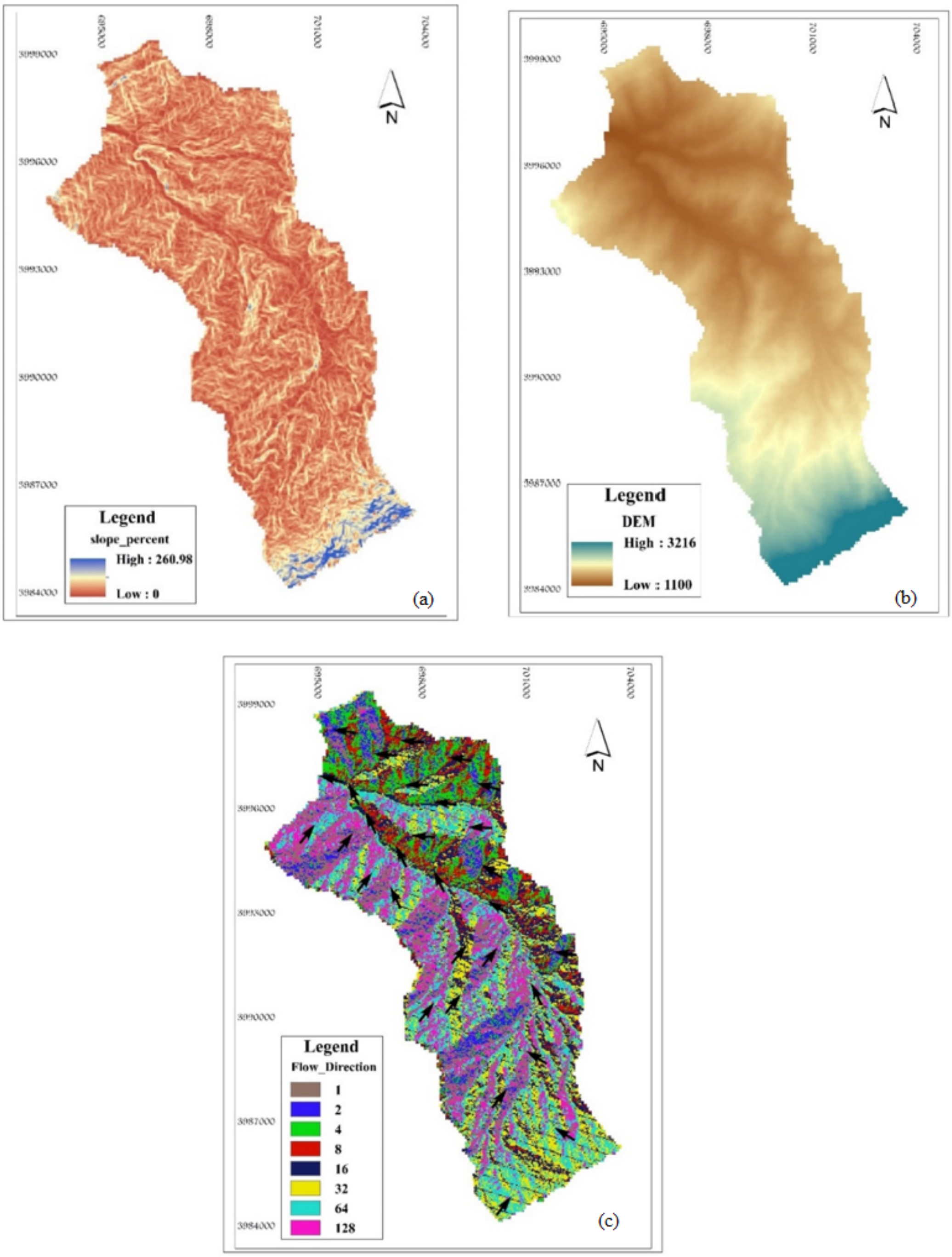

Figure 8 - Kasilian catchment: a) local slope, b) DEM, and c) flow direction

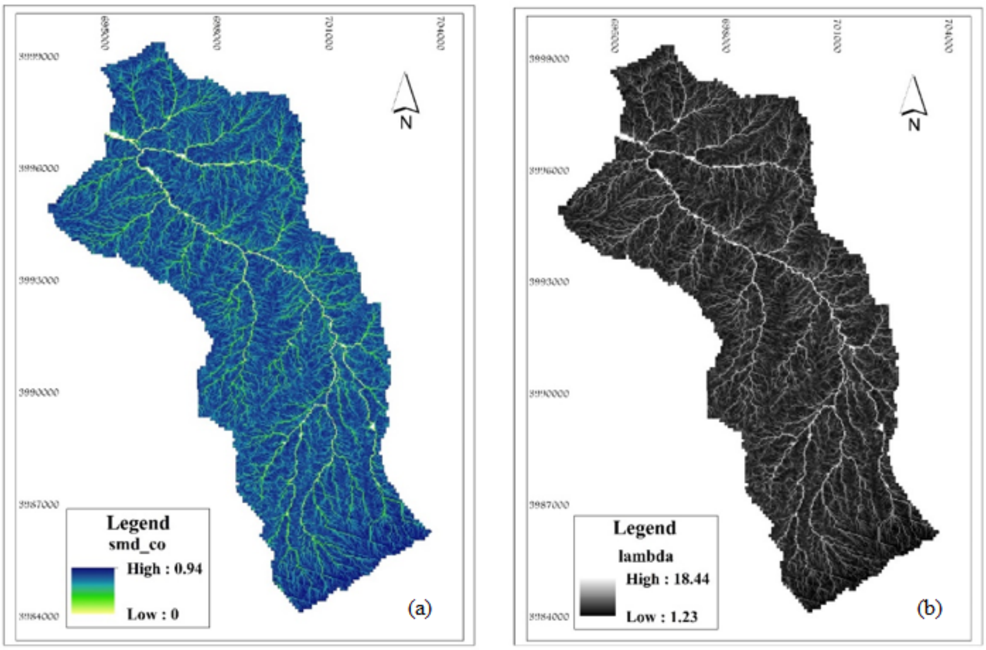

Figure 9 - Variation of a) SMD (m), and b) λ over the Kasilian catchment

Based on the calculated SMD values across the catchment, variations in the CN parameter can be assessed as a pivotal determinant in hydrological computations, as delineated in Equation (12) (see Figure 10). Theoretically ranging from 0 to 100, CN values in practice exhibit a narrower range. Soils characterized by vegetative cover, coarse grains, and high permeability tend to exhibit CN values closer to 10, indicative of enhanced infiltration capacity, whereas CN approaches 100 in soils with low permeability, promoting greater surface runoff.

Figure 10 illustrates the spatial distribution of CN values within the catchment, ranging from 21.3 to 100. Notably, CN values approaching 100 are observed in downstream regions proximal to streams, underscoring the heightened saturation propensity in these areas, where SMD values are also minimized. Furthermore, Figure 11 delineates the spatial variation in accumulated infiltration depths for rainfall depths of 5 and 20 mm (P = 5 and 20 mm), calculated according to Equation (13). These visualizations offer valuable insights into the spatial dynamics of infiltration across the catchment under varying rainfall scenarios.

Accordingly, if $P \leq 0.2\ D_i$, the amount of cumulative infiltration will be the same as the amount of rainfall $(F_t = P)$. On the other hand, if $P > 0.2\ D_i$ (when the rainfall depth P is greater than the initial reserve), then the cumulative infiltration should be calculated.

As shown in Figure 11, the initial infiltration rate (I_a) is high for rainfall of 5 and 20 mm at the upstream parts of the catchment (in comparison with that in the rivers) and the total rainfall infiltrates and thus, $F = P$. However, the soil becomes saturated in downstream parts (near rivers) of the hillslopes and thus, the surface runoff is generated and the infiltration decreases and tends to zero. The change in infiltration from $F_t = P$ to $F_t = 0$ occurs at the catchment surface in proportion to the changes in SMD and CN.

In this research, the amount of rainfall between 5 and 20 mm was considered. These unrealistic values are based on the average rainfall of the region . Figure 12 illustrates the variation of the RC in the Kasilian catchment for 20 mm rainfall.

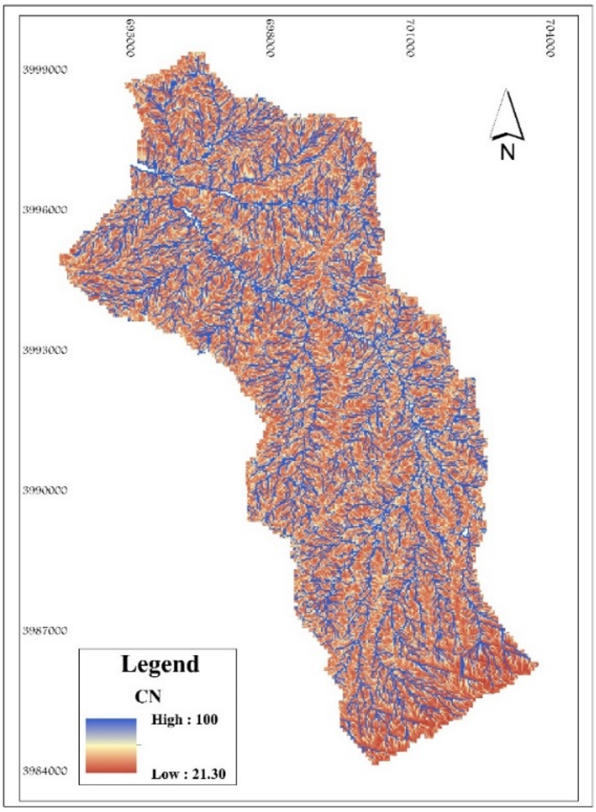

Figure 10 - Variation of CN in Kasilian catchment

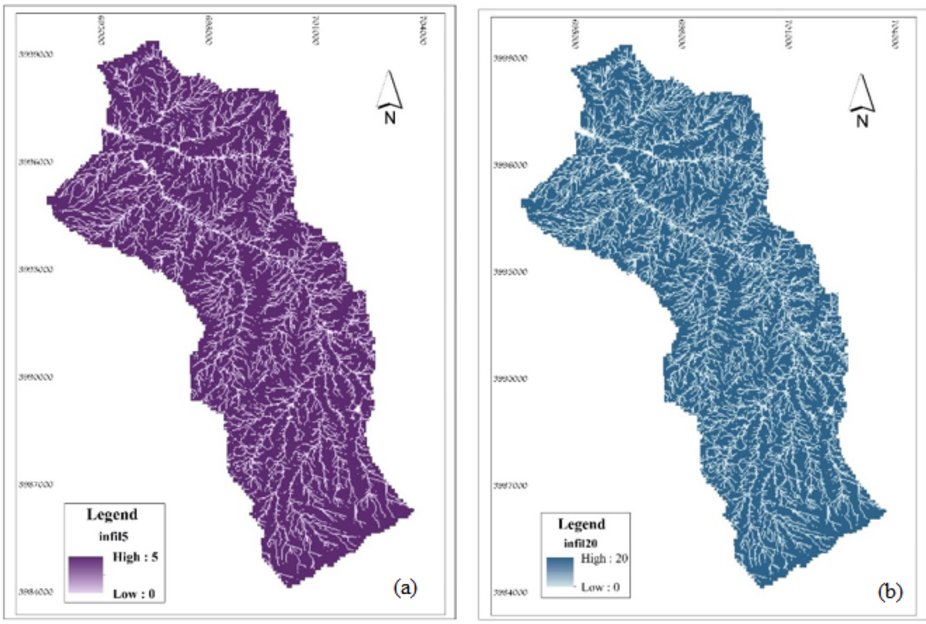

Figure 11 - Spatial changes of the infiltration (mm) in the Kasilian catchment for: a) rainfall depth = 5 mm, and b) rainfall depth = 20 mm

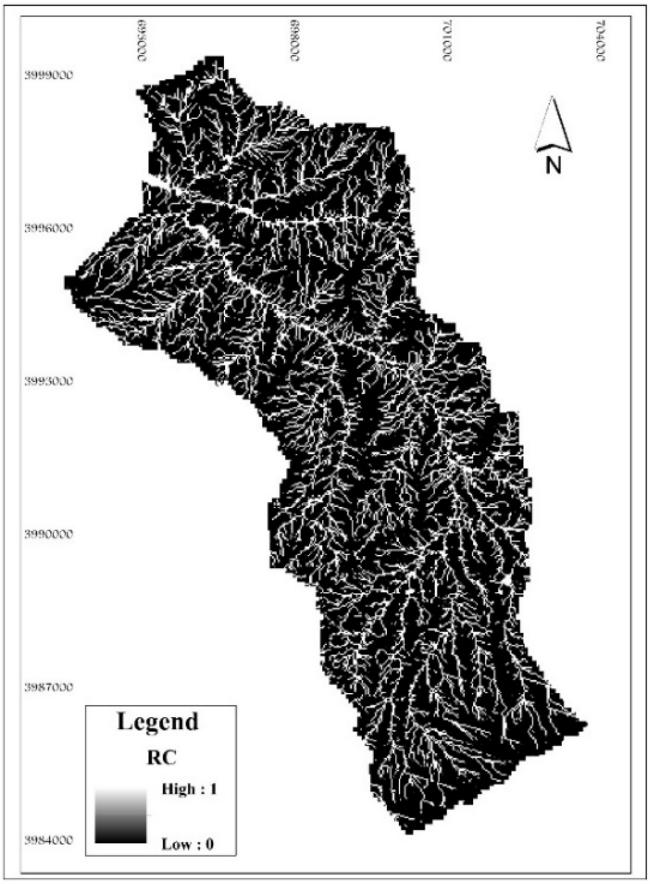

Figure 12 - Spatial variation of RC in Kasilian catchment

As depicted in Figure 12, the RC exhibits a discernible spatial pattern within the catchment. At pixels distant from waterways, RC tends towards 0, indicating a lack of runoff capacity potential at these locations. Consequently, rainfall at these points predominantly infiltrates into the soil without generating significant surface runoff. Conversely, RC values near waterways approach 1, indicative of heightened runoff generation in response to rainfall events. This spatial distribution of RC across the catchment serves as a practical and essential tool for estimating flood volumes, offering valuable insights into the hydrological response of the landscape to precipitation inputs.

Temporal changes in infiltration (laboratory model)

Figure 13 shows the temporal and spatial variations of the infiltration along the hillslope at different times of t = 0, 1, 2 and 3 hours from the beginning of rainfall according to Eq. (23).

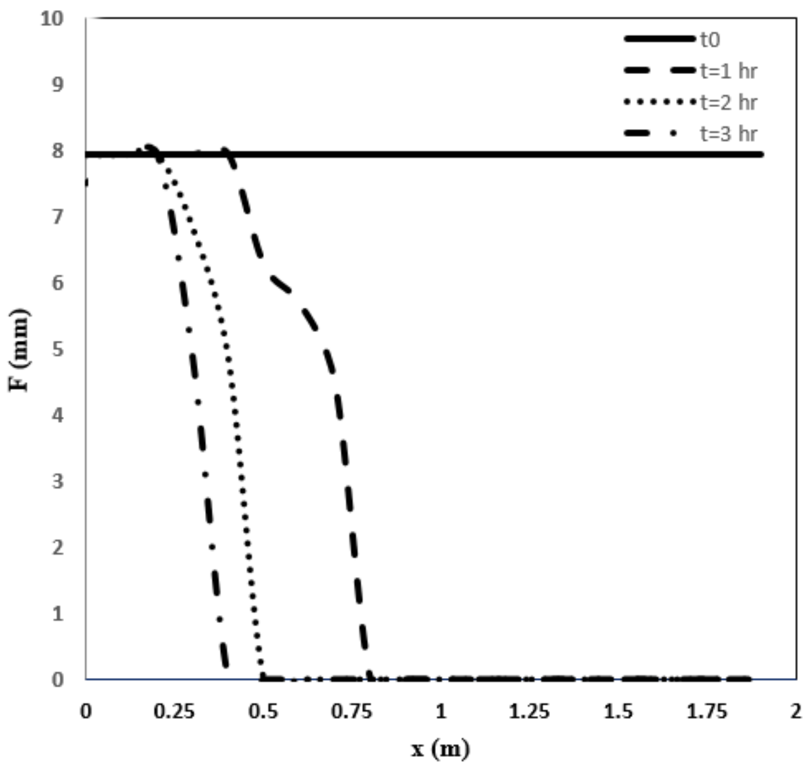

Figure 13 - Variation of the depth of cumulative infiltration (F) over time along the hillslope(X)

As observed, the temporal evolution of infiltration along the hillslope exhibits a decreasing trend over time, ultimately reaching complete cessation towards the downstream regions. This observation indicates a progressive increase in hillslope saturation from downstream to upstream locations. For instance, at t = 1 hr (one hour elapsed), infiltration ceases approximately 0.75 m from the slope's exit point, encompassing roughly 60% of the slope's length. Similarly, at t = 3 hr (three hours elapsed), infiltration halts approximately 0.4 m from the slope's exit point, covering around 80% of the slope's length.

Consequently, precipitation in these areas is entirely converted into runoff, signifying the transition from infiltration-dominated to runoff-dominated hydrological regimes. In the initial conditions (t = 0), infiltration depth is assumed to equal the rainfall depth, resulting in complete rainfall penetration along the slope.

Figure 14 delineates the temporal variations in RC along the slope at four distinct time intervals, as calculated using Equation (24). This visualization offers insights into the dynamic evolution of runoff generation along the hillslope over time, providing valuable information for understanding the temporal dynamics of hydrological processes within the study area.

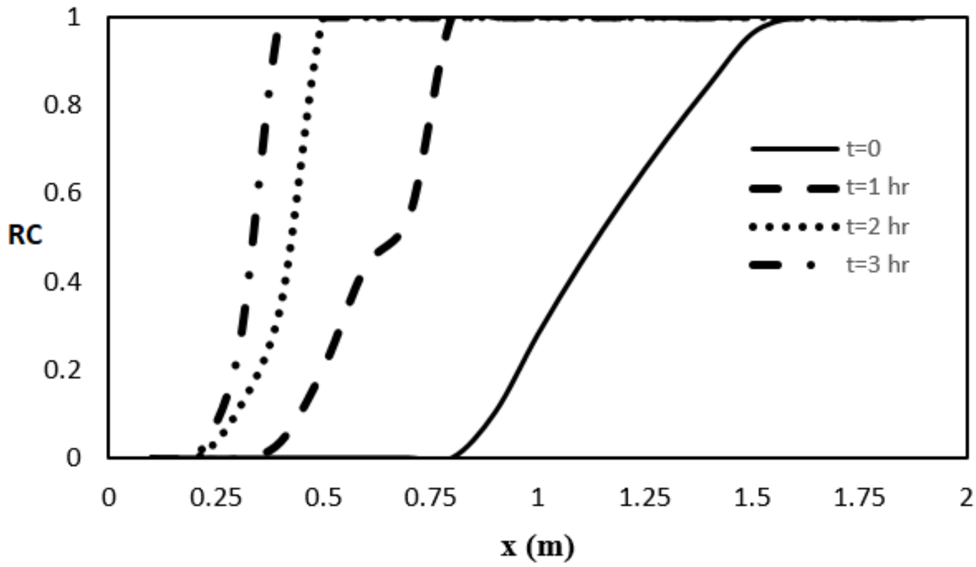

Figure 14 - Changes in runoff coefficient (RC) over time along the slope

As evident from the observations, downstream segments of the hillslope exhibit a greater degree of saturation, accompanied by RC values nearing unity within these regions. This saturation process coincides with a reduction in soil permeability, leading to heightened surface runoff generation and, consequently, RC values approaching 1. Over time, RC values progressively converge towards 1 across a broader expanse of the hillslope, indicative of the enhanced runoff-generating capacity of the terrain.

Figure 15 illustrates the temporal evolution of CN values along the hillslope at four distinct time intervals, computed using Equation (25). As depicted, CN values tend towards 100 in the majority of hillslope regions over time, reflecting widespread soil saturation. Specifically, at t = 3 hr, approximately 90% of the hillslope exhibits CN values of 100, signifying saturation propagation from downstream to upstream regions. These findings suggest a direct relationship between CN and RC, wherein higher CN values correspond to increased runoff potential, aligning with the observed trends in RC dynamics along the hillslope.

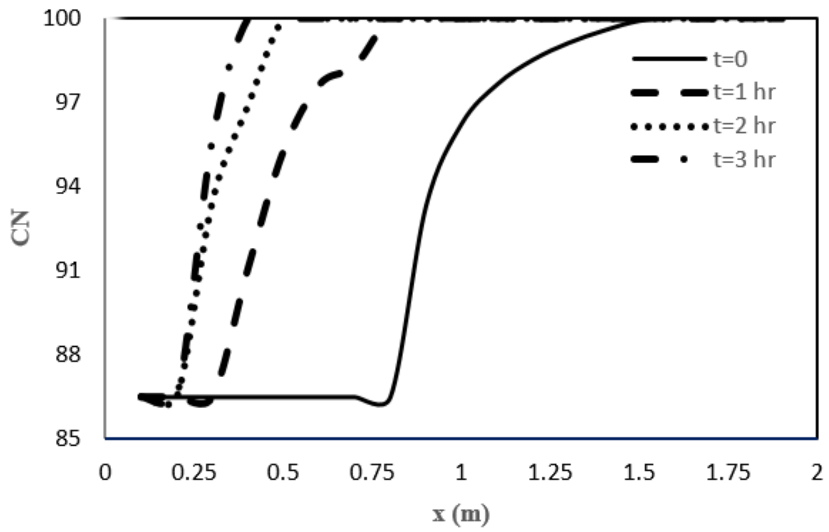

Figure 15 - Changes in the curve number (CN) over time along the hillslope

DOI: 10.36253/jaeid-15137

This section presents an in-depth analysis of the runoff hydrograph derived through the application of the TOPMODEL method. Figure 16 illustrates the ascending branch of the total observed runoff, encompassing both surface and subsurface components, across the laboratory hillslope under investigation. The runoff hydrograph was generated using the methodology proposed in this study (Eqs. 21 and 22) for a continuous rainfall duration spanning 5 hours, with a corresponding rainfall intensity of 31.73 mm/hr.

The results demonstrate a high degree of consistency between the simulated runoff derived from the proposed methodology and the observed data, with errors deemed acceptable within the scope of the analysis. This alignment between simulation outcomes and observational data underscores the efficacy and reliability of the methodology employed in this research for predicting runoff dynamics within the laboratory hillslope setting.

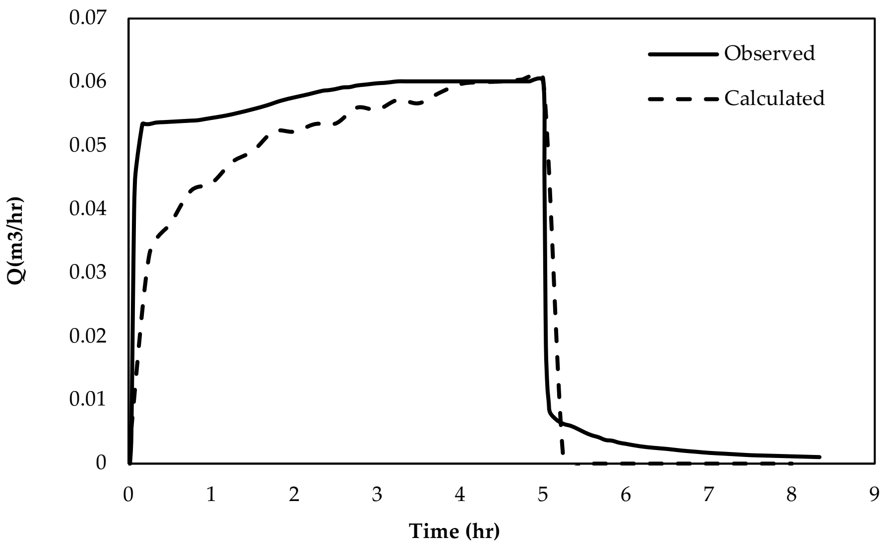

Figure 16 - Comparison of total observational and computational runoff (for 9-degree slope, duration 5 hr and 31.73 mm/hr rainfall intensity)

A comparison between observed runoff and calculated runoff based on Nash-Sutcliffe Efficiency coefficient of efficiency (CE), Peak Error (PE), and Root Mean Square Error (RMSE) metrics is presented in Table 2.

The Nash-Sutcliffe coefficient of efficiency (CE) stands as a prevalent indicator employed for assessing the efficacy of hydrological models. CE, PE and RMSE are calculated according Eqs. from 32 to 34:

$$CE = 1 - \frac{\sum_{t=1}^{n}[Q_o - Q_s]^2}{\sum_{t=1}^{n}[Q_o - \overline{Q_o}]^2} \quad (32)$$

$$PE = 100 \times [Q_{p_s} - Q_{p_o}]/Q_{p_o} \quad (33)$$

$$RMSE = \left[\frac{1}{n}\sum_{i=1}^{n}(Q_o - Q_s)^2\right]^{0.5} \quad (34)$$

where Q_O is the observed discharge at time t; Q_s is the simulated discharge at time t; $\overline{Q_o}$ is the average observed discharge during the storm event; n is the number of discharge records during the storm event; Q_{p_s} is the peak discharge of the simulated hydrograph and Q_{p_o} is the observed peak discharge.

Table 2 - The result of the validation criteria of runoff

Criteria	Result
CE	0.979
PE	-1.51%
RMSE	0.00239

The value of CE=0.979 is close to 1 and the value of PE=1.51% is a low error that shows the accuracy of the calculations.

Conclusion

The examination of spatial and temporal distribution patterns of infiltration and runoff within catchments presents a significant challenge in hydrological modeling. For instance, while the Soil Conservation Service Curve Number (SCS-CN) infiltration model provides insights into infiltration dynamics at various points within a catchment for a single event, its efficacy hinges on parameters such as antecedent soil moisture and land use, predominantly operating under the Hortonian mechanism for runoff generation. Conversely, the TOPMODEL model, functioning as a subsurface flow model, primarily operates under the Dunne-block mechanism, predicting moisture spatial distribution within catchments.

Integrating these two models offers hydrologists a more comprehensive and accurate understanding of spatial infiltration and runoff dynamics, particularly pertinent in ungauged catchments prevalent in developing countries. Leveraging Geographic Information Systems (GIS) facilitates enhanced evaluation of spatial infiltration changes and associated parameters.

To achieve this objective, we amalgamated the SCS-CN and TOPMODEL models. Initially, infiltration equations were extended to compute cumulative infiltration values, Runoff Coefficient (RC), and Curve Number (CN) parameters, enabling characterization of spatial changes across the catchment over time intervals. Subsequently, data from the Kasilian catchment in Iran were utilized to assess the spatial distribution of infiltration and its parameters.

Employing the proposed model in conjunction with GIS, we scrutinized the spatial variation of CN and RC within the catchment, revealing CN values spanning from 21.3 to 100, with higher CN values near saturated areas, indicative of increased surface runoff potential. Concurrently, infiltration diminishes, and RC approaches unity in proximity to saturated regions.

Moreover, Dynamic TOPMODEL facilitates the exploration of temporal variations in soil moisture within the catchment. Coupled with the SCS-CN infiltration model, this integration enables examination of both spatial and temporal infiltration changes along hillslopes.

Finally, equilibrium equations were incorporated into the TOPMODEL model to calculate variations in the Soil Moisture Deficiency (SMD) parameter over time intervals. To support these analyses, a rainmaking laboratory model was employed to assess spatial changes in infiltration time, CN, and RC along the laboratory hillslope, providing valuable insights into runoff dynamics under controlled conditions.

List of symbols

Abbreviation	Definition
SMD	soil moisture deficit
RC	runoff coefficient
CN	curve number
TWI	topographic wetness index
λ	topographic wetness index
$\overline{\lambda}$	average λ
a	specific catchment area
D_i	SMD to saturated condition at point i
$\overline{D}$	mean SMD
Θ_e	effective soil moisture
f	Decay factor
m	$\Theta e / f$
P	rainfall depth
I_a	initial loss
R	excess rainfall
F	cumulative infiltration
S	potential maximum soil moisture retention
Θ_i	initial soil moisture
q_i	interflow corresponding to an area drained per unit contour length
A_c	contributing area to the surface runoff
z_i	moisture deficit to saturated condition and the potential for water retention in the soil
C_i	value of RC in each element
w_i	with flow
Q_v	recharge rate of the unsaturated zone from saturated zone over the time interval t
Q_B	outflow from the subsurface store into the channel over the time interval t and t+Δt
A	area of the hillslope
Δt	time interval
K_0	hydraulic conductivity coefficient at the ground surface
T_0	soil transmissivity
α_i	area draining through locatIon i per unit contour length
V	runoff volume
I	represents the rainfall intensity
Q_{Direct}	direct runoff
$\tan \beta$	local surface slope
β	slope angle
s	Slope
SCS-CN	Soil Conservation Service Curve Number

TOPMODEL	TOPography based hydrological MODEL

References

Adnan, R. M., Petroselli, A., Heddam, S., Guimarães Santos, C. A., & Kisi, O. (2021a). Comparison of different methodologies for rainfall-runoff modeling: machine learning vs conceptual approach. *Natural Hazards*, *105*, 2987–3011.

Adnan, R.M., Petroselli, A., Heddam, S., Guimarães Santos, C.A., & Kisi, O. (2021b). Short term rainfall-runoff modeling using several machine learning methods and a conceptual event-based model. *Stochastic Environmental Research and Risk Assessment, 35*, 597-616.

Apollonio, C., Delle Rose, M., & Fidelibus, C. (2018). Water management problems in a karst flood-prone endorheic basin. *Environmental Earth Sciences, 77*, 676.

Apollonio, C., Petroselli, A., Tauro, F., Cecconi, M., Biscarini, C., Zarotti, C., & Grimaldi, S. (2021). Hillslope erosion mitigation: An experimental proof of a nature-based solution. *Sustainability, 13*(11), 6058.

Ayalew, D. W., Petroselli, A., De Luca, D. L., & Grimaldi, S. (2022). An evidence for enhancing the design hydrograph estimation for small and ungauged basins in Ethiopia. *Journal of Hydrology: Regional Studies, 42,* 101123.

Azizian, A., & Shokoohi, A. (2015). Effects of data resolution and stream delineation threshold area on the results of a kinematic wave based GIUH model. *Water SA, 41*(1), 61-70.

Azizian, A., & Shokoohi, A. (2019). Development of a new method for estimating SCS curve number using TOPMODEL concept of wetness index (case study: Kasilian and Jong watersheds, Iran). *Acta Geophysica, 67*(4), 1163-1177.

Bales, J., & Betson, R. P. (1981). The curve number as a hydrologic index. In *Rainfall-runoff relationships* (pp. 371–386).

Beven, K.J. (2011). *Rainfall-runoff modelling: the primer*. John Wiley & Sons.

Beven, K.J. (1997). TOPMODEL: A critique. *Hydrological Processes, 11,* 1069-1085.

Beven, K. J., & Wood, E. F. (1983). Catchment geomorphology and the dynamics of runoff contributing areas. *Journal of Hydrology, 65*, 139-158.

Beven, K. J. (1986). Runoff production and flood frequency in catchments of order n: An alternative approach. In V. K. Gupta, I. Rodriguez-Iturbe, & E. F. Wood (Eds.), *Scale problems in hydrology*. D. Reidel.

Boughton, W. C. (1987). Evaluating partial areas of watershed runoff. *Journal of Irrigation and Drainage Engineering, 113*(3), 356-366.

Carrillo, F., Soares, J. V., Ferreira, N. J., & Rodriguez, D. A. (2006). Runoff coefficient and its relation to phytogeography in Brazil. *Proceedings of the 8th International Conference on Small Hydropower and Management of Water Resources (ICSHMO)*, Foz do Iguaçu, Brazil, April 24–28, 2006, 229–233.

Cerdan, O., Le Bissonnais, Y., Govers, G., Lecomte, V., Van Oost, K., Couturier, A., ... & Dubreuil, N. (2004). Scale effect on runoff from experimental plots to catchments in agricultural areas in Normandy. *Journal of hydrology, 299*(1-2), 4-14.

Chairat, S., & Delleur, J. W. (1993). Integrating a physically based hydrological model with GRASS. *IAHS Publications, 143*, 143–143.

Chow, V. T. (1964). *Handbook of Applied Hydrology*. McGraw-Hill.

Crimaldi, M., & Lama, G. F. C. (2021). Impacts of riparian plants biomass assessed by UAV-acquired multispectral images on the hydrodynamics of vegetated streams. *Proceedings of the 29th European Biomass Conference and Exhibition*, 26–29 April 2021, Online, 1157–1161.

Dos Reis Castro, N. M., Auzet, A. V., Chevallier, P., & Leprun, J. C. (1999). Land use change effects on runoff and erosion from plot to catchment scale on the basaltic plateau of Southern Brazil. *Hydrological Processes, 13*(11), 1621-1628.

Eldridge, D. J., Wang, L., & Ruiz-Colmenero, M. (2015). Shrub encroachment alters the spatial patterns of infiltration. *Ecohydrology, 8*(1), 83-93.

Faouzi, E., Arioua, A., Hssaisoune, M., Boudhar, A., Elaloui, A., & Karaoui, I. (2022). Sensitivity analysis of CN using SCS-CN approach, rain gauges and TRMM satellite data assessment into HEC-HMS hydrological model in the upper basin of Oum Er Rbia, Morocco. *Modeling Earth Systems and Environment, 8*(4), 4707-4729.

Fariborzi, H., Sabzevari, T., Noroozpour, S., & Mohammadpour, R. (2019). Prediction of the subsurface flow of hillslopes using a subsurface time-area model. *Hydrogeology Journal, 27*(4), 1401-1417.

Franchini, M., Wendling, J., Obled, Ch., & Todini, E. (1996). Physical interpretation and sensitivity analysis of the TOPMODEL. *Journal of Hydrology, 175*, 293-338.

Gottschalk, L., & Weingartner, R. (1998). Distribution of peak flow derived from a distribution of rainfall volume and runoff coefficient, and a unit hydrograph. *Journal of hydrology, 208*(3-4), 148-162.

Gupta, V.K., Waymire, E., & Wang, C.T. (1980). Representation of an instantaneous unit hydrograph from geomorphology. *Water Resources Research, 16* (5), 855–862.

Ismail, M. M., Abd-Ulkareem, F. A., & Hussain, T. A. (2021). Computation of Climatic Water Balance of AL-Sulaymania Meteorological Station for the Period 1980-2016, Kurdistan Region, Northeast of Iraq. *Engineering and Technology Journal, 39*(12), 1952-1959.

Jaynes, D. B., & Hunsaker, D. J. (1989). Spatial and temporal variability of water content and infiltration on a flood irrigated field. *Transactions of the ASAE, 32*(4), 1229-1238.

Lama, G. F. C., & Crimaldi, M. (2021). Assessing the role of gap fraction on the leaf area index (LAI) estimations of riparian vegetation based on fisheye lenses. *Proceedings of the 29th European Biomass Conference and Exhibition*, 26–29 April 2021, Online, 1172–1176.

Lama, G. F. C., Crimaldi, M., De Vivo, A., Chirico, G. B., & Sarghini, F. (2021). Eco-hydrodynamic characterization of vegetated flows derived by UAV-based imagery. *Proceedings of the 2021 IEEE International Workshop on Metrology for Agriculture and Forestry (MetroAgriFor)*, 273–278.

Lamb, R., Beven, K., & Myrabø, S. (1997). Discharge and water table predictions using a generalised TOPMODEL formulation. *Hydrological Processes, 11*(9), 1145-1167.

Li, Z.J., & Zhang, K. (2008). Comparison of three GIS-based hydrological models. *Journal of Hydrologic Engineering, 13*(5), 364-370.

Longobardi, A., Villani, P., Grayson, R. B., & Western, A. W. (2003). On the relationship between runoff coefficient and catchment initial conditions. *Proceedings of MODSIM*, 867–872.

Merz, R., Blöschl, G., & Parajka, J. (2006). Spatio-temporal variability of event runoff coefficients. *Journal of Hydrology, 331*(3-4), 591-604.

Merz, R., & Blöschl, G. (2009). A regional analysis of event runoff coefficients with respect to climate and catchment characteristics in Austria. *Water Resources Research, 45*(1).

Mesa, O. J., & Mifflin, E. R. (1986). On the relative role of hillslope and network geometry in hydrologic response. In V. K. Gupta, I. Rodriguez-Iturbe, & E. F. Wood (Eds.), *Scale problems in hydrology* (pp. 1–17). D. Reidel.

McCuen, R. H. (1982). *A guide to hydrologic analysis using SCS methods*. Prentice-Hall.

Michel, C., Vazken, A., & Perrin, C. (2005). Soil conservation service curve number method: How to mend a wrong soil moisture accounting procedure? *Water Resources Research, 41*(2), 1–12.

Mishra, S.K., Sahu, R.K., Eldho, T.I., & Jain, M.K. (2006). An improved I a S relation incorporating antecedent moisture in SCS-CN methodology. *Water Resources Management, 20*(5), 643-660.

Montgomery, D.R., & Dietrich, W.E. (1994). A physically based model for the topographic control on shallow landsliding. *Water Resources Research, 30*(4), 1153-1171.

Mohammadpour, R., Ghani, A. A., Sabzevari, T., & Fared Murshed, M. (2021). Local scour around complex abutments. *ISH Journal of Hydraulic Engineering, 27*(sup1), 165-173.

Nachabe, M. H. (2006). Equivalence between TOPMODEL and the NRCS curve number method in predicting variable runoff source areas 1. *Journal of the American Water Resources Association, 42*(1), 225-235.

Naden, P. (1992). Spatial variability in flood estimation for large catchments: the exploitation of channel network structure. *Hydrological Sciences Journal, 37* (1), 53–71.

Noto, S., Tauro, F., Petroselli, A., Apollonio, C., Botter, G., & Grimaldi, S. (2022). Low cost stage-camera system for continuous water level monitoring in ephemeral streams. *Hydrological Sciences Journal 67*(9), 1439-1448.

Nourani, V., Roughani, A., & Gebremichael, M. (2011). TOPMODEL capability for rainfall-runoff modeling of the Ammameh watershed at different time scales using different terrain algorithms. *Journal of Urban and Environmental Engineering, 5*(1), 1-14.

Ogbozige, F. J. (2022). Development of Intensity-Duration-Frequency (IDF) Models for Manually Operated Rain Gauge Catchment: A Case Study of Port Harcourt Metropolis Using 50 years Rainfall Data. *Engineering and Technology Journal, 40*(05), 627-635.

Ou, Y. (2009). *Hydrological modeling in the Marmot Creek basin* (Doctoral dissertation, Memorial University of Newfoundland).

Patil, S., & Bardossy, A. (2006). Regionalization of runoff coefficient and parameters of an event based Nash-cascade model for predictions in ungauged basins. *Geophysical Research Abstracts*, 8, 74.

Panjabi, K., Rudra R., Goel P., Daggupati P., Kumar Shrestha N., Shukla R., Zhang B., & Allataifeh N. (2020). Mapping runoff generating areas using AGNPS-VSA model. *Hydrological Sciences Journal, 65*(13), 2224-2232.

Petroselli, A., Asgharinia, S., Sabzevari, T., & Saghafian, B. (2020). Comparison of design hydrograph estimation methods for ungauged basins in Iran. *Hydrological Sciences Journal, 65*(1), 127-137.

Pirone, D., Cimorelli, L., Del Giudice, G., & Pianese, D. (2022). Short-term rainfall forecasting using cumulative precipitation fields from station data: A probabilistic machine learning approach. *Journal of Hydrology, 128*, Article 128949.

Pishvaei, M. H., Sabzevari, T., Noroozpour, S., & Mohammadpour, R. (2020). Effects of hillslope geometry on spatial infiltration using the TOPMODEL and SCS-CN models. *Hydrological Sciences Journal, 65*(2), 212-226.

Quinn, P.F., Ostendorf, B., Beven, K., & Tenhunen, J. (1998). Spatial and temporal predictions of soil moisture patterns and evaporative losses using TOPMODEL and the GASFLUX model for an Alaskan catchment. *Hydrology and Earth System Sciences, 2*, 51-64.

Rinaldo, A., Marani, A., & Rigon, R. (1991). Geomorphological dispersion. *Water Resources Research, 27*, 513–525.

Rodriguez-Iturbe, I., & Valdes, J.B. (1979). The geomorphologic structure of hydrologic response. *Water Resources Research, 15*, 1409–1420.

Rodriguez-Iturbe, I., Gonzalez-Sanabria, M., & Bras., R.L. (1982). A geomorphoclimatic theory on the instantaneous unit hydrograph. *Water Resources Research, 18* (4),877–886.

Rodríguez-Iturbe, I., & Rinaldo, A. (1997). *Fractal river networks: chance and self-organization*. Cambridge: Cambridge University Press.

Rodríguez-Blanco, M. L., Taboada-Castro, M. M., & Taboada-Castro, M. T. (2012). Rainfall–runoff response and event-based runoff coefficients in a humid area (northwest Spain). *Hydrological Sciences Journal, 57*(3), 445-459.

Soomro, A. G., Babar, M. M., Memon, A. H., Zaidi, A. Z., Ashraf, A., & Lund, J. (2019). Sensitivity of direct runoff to curve number using the SCS-CN method. *Civ. Eng. J, 5*, 2738-2746.

Sabzevari, T., Ardakanian, R., Shamsaee, A., & Talebi, A. (2009). Estimation of flood hydrograph in no statistical watersheds using HEC-HMS model and GIS (Case study: Kasilian watershed). *J. Water Eng, 4*, 1-11.

Sabzevari, T. (2010). *Development of catchments geomorphological instantaneous unit hydrograph based on surface and subsurface flow response of complex hillslopes* (Doctoral dissertation). Islamic Azad University.

Sabzevari, T. (2017). Runoff prediction in ungauged catchments using the gamma dimensionless time-area method. *Arabian Journal of Geosciences, 10*, 1-11.

Sherman, L. K. (1932). Streamflow from rainfall by the unit-graph method. *Engineering News Record, 108*, 501-505.

Singh, P.K., Gaur, M.L., Mishra, S.K., & Rawat, S.S. (2010). An updated hydrological review on recent advancements in soil conservation service-curve number technique. *Journal of Water and Climate Change, 1*(2), 118-134.

SCS, *National engineering handbook. Hydrology Section*, 4. (1972).

Shokoohi, A. (2016). Effect of Data Resolution on Topographic Index and Performance of the Simi-Distributed Model: TOPMODEL. *Modares Civil Engineering Journal, 16*(2), 187-201.

Sisi, L., Gitau, M., Engel, B.A., Zhang, L., Du, Y., Wallace C., & Flanagan, D.C. (2017). Development of a distributed hydrological model to facilitate watershed management. *Hydrological Sciences Journal, 62*(11), 1755-1771.

Sivapalan, M., Beven, K., & Wood, E. F. (1987). On hydrologic similarity: 2. A scaled model of storm runoff production. *Water Resources Research, 23*(12), 2266-2278.

Son, N., & Bouvier C. (2019). Flood modelling using the distributed event-based SCS-LR model in the Mediterranean Real Collobrier catchment. *Hydrological Sciences Journal, 64*(11), 1351-1369.

Stuart, N., & Stocks, C. (1993). Hydrological modelling within GIS: An integrated approach. *IAHS Publication, 319*, 319.

Tauro, F., Petroselli, A., Porfiri, M., Giandomenico, L., Bernardi, G., Mele, F., ... & Grimaldi, S. (2016). A novel permanent gauge-cam station for surface-flow observations on the Tiber River. *Geoscientific Instrumentation, Methods and Data Systems, 5*(1), 241-251.

Tricker, A. S. (1981). Spatial and temporal patterns of infiltration. *Journal of Hydrology, 49*(3-4), 261-277.

Takeuchi, K., Hapuarachchi, P., Zhou, M., Ishidaira, H., & Magome, J. (2008). A BTOP model to extend TOPMODEL for distributed hydrological simulation of large basins. *Hydrological Processes, 22*(17), 3236–3251.

Takeuchi, K., Tianqi, A., & Ishidaira H. (1999). Introduction of block-wise use of TOPMODEL and Muskingum-Cunge method for the hydroenvironmental simulation of a large ungauged basin. *Hydrological Sciences Journal, 44*(4), 633-646.

Visessri, S., & McIntyre, N. (2016). Regionalisation of hydrological responses under land-use change and variable data quality. Hydrological Sciences Journal, 61(2), 302-320.

Woods, R. A., Sivapalan, M., & Robinson, J. S. (1997). Modeling the spatial variability of subsurface runoff using a topographic index. *Water Resources Research, 33*(5), 1061-1073.

Wang, G., Hapuarachchi, H. A. P., Takeuchi, K., & Ishidaira, H. (2010). Grid-based distribution model for simulating runoff and soil erosion from a large-scale river basin. *Hydrological Processes: An International Journal, 24*(5), 641-653.

Western, A. W., Grayson, R. B., Blöschl, G., Willgoose, G. R., & McMahon, T. A. (1999). Observed spatial organization of soil moisture and its relation to terrain indices. *Water resources research, 35*(3), 797-810.

Wolock, D. M., & Price, C. V. (1994). Effects of digital elevation model map scale and data resolution on a topography-based watershed model. *Water Resources Research, 30*(11), 3041-3052.